Hindawi Publishing Corporation
Journal of Sensors
Volume 2016, Article ID 5185242, 9 pages
http://dx.doi.org/10.1155/2016/5185242

Research Article

Characteristics of Relocated Quiet Zones Using Virtual Microphone Algorithm in an Active Headrest System

Seokhoon Ryu and Young-Sup Lee

Department of Embedded Systems Engineering, Incheon National University, 119 Academy-ro, Yeonsu-gu, Incheon 406-772, Republic of Korea

Correspondence should be addressed to Young-Sup Lee; ysl@inu.ac.kr

Received 30 January 2016; Accepted 30 March 2016

Academic Editor: Yurong Qian

This study displays theoretical and experimental investigation on the characteristics of the relocated zone of quiet by a virtual microphone (VM) based filtered-x LMS (FxLMS) algorithm which can be embedded in a real-time digital controller for an active headrest system. The attenuation changes at the relocated zones of quiet by the variation of the distance between the ear and the error microphone are mainly examined. An active headrest system was implemented for the control experiment at a chair and consists of two (left and right) secondary loudspeakers, two error microphones, two observer microphones at ear positions in a HATS, and other electronics including a dSPACE 1401 controller. The VM based FxLMS algorithm achieved an attenuation of about 22 dB in the control experiment against a narrowband primary noise by the variation of the distance between the ear and the error microphone. The important factors for the algorithm are discussed as well.

1. Introduction

With the advancement of the embedded processors, active noise control (ANC) to cancel an unwanted noise with antinoise by taking the principle of superposition has been studied in many industrial applications [1–5]. In particular, in the case of a vehicle engine, the adaptive feedforward algorithms such as the FxLMS (filtered-reference least mean square) have been applied successfully to actively control a narrowband interior noise in a car cabin generated by the engine [2, 3, 5]. In terms of noise suppression performance, although the global reduction of the engine noise in a car cabin is ideal, this leads to excessive increase of cost, weight, occupancy, and so forth. For this reason, it can be even more efficient to develop local quiet zones [2, 5, 6] near the headrest of chairs. Although the local quiet zone is successfully generated at the location, the head movement in the headrest is restricted due to error microphones near the secondary loudspeaker under the FxLMS approach.

The virtual microphone (VM) technique that relocates the zone of quiet generated at an error microphone to the position of a virtual microphone is introduced to minimize the signal at the virtual microphone [6–9]. Elliott and David suggested a virtual microphone method for local ANC [6]; likewise Roure and Albarrazin showed a remote microphone technique for ANC [7]. Pawelczyk investigated the multiple adaptive feedback algorithm for active headrest [8] and Moreau et al. reviewed virtual sensing algorithms in ANC [9]. Also a feedback multichannel minimum-variance virtual microphone active noise control system for active headrest system was investigated [10]. Das et al. carried out a remote microphone algorithm using an internal model without using reference microphone [11]. From these studies, the quiet zone formed at the error microphone can be shifted to the ear position by the VM sensing algorithm.

In this paper theoretical and experimental investigation on the characteristics of the relocated zone of quiet by a VM based FxLMS algorithm which can be embedded in a real-time digital controller for an active headrest system is considered against the narrowband swept primary noise such as accelerating car engine noise. The properties of the attenuations and responses at the relocated zones of quiet with the variation of the distance between the observer microphone at the ear position and the error microphone are analyzed in depth. In addition, the governing factors of the VM based FxLMS, such as the secondary path and the virtual

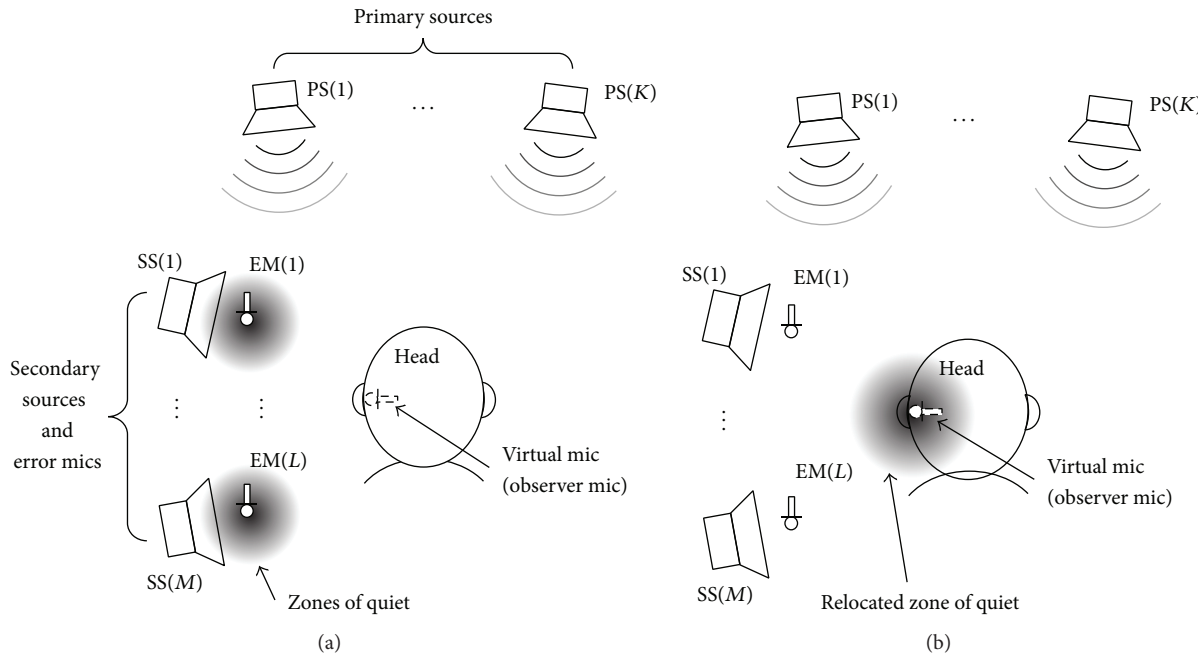

Figure 1: Localization of the quiet zone by an active method. (a) Location of the quiet zones at error microphones (VM algorithm off). (b) Relocation of the quiet zone at the ear position (VM algorithm on).

secondary path models, are clarified and their effects are analyzed. The effect of the inclusion of the response difference in the algorithm, which will be symbolized as $\widehat{V}(z)$ in the main text, between the error microphone and the observer microphone by the primary source is discussed to provide better understanding of the VM based algorithm.

The rest of this paper is organized as follows. In Section 2, theoretical considerations are described to derive proper equations for relocating the quiet zone using the VM based FxLMS algorithm. Section 3 presents the experimental setup including the implementation of the active headrest system, the modelling of the secondary and virtual secondary paths, and the property of the narrowband primary noise. Intensive analysis and discussion from the measured results of the real-time control are written in Section 4. Also, the characteristics of the relocated quiet zones generated by the VM based FxLMS algorithm are discussed in the same section. Finally, conclusions are summarized in Section 5.

2. Relocation of Active Quiet Zone Using VM Based FxLMS Algorithm

In this section, the FxLMS algorithm and the VM based FxLMS algorithm are discussed for generating a quiet zone at the position of an error microphone and relocating the quiet zone to the point of a virtual microphone, respectively, in a headrest system.

As illustrated in Figure 1, the active quiet zone around a headrest can be relocated from the error microphone (near to the secondary loudspeaker) to the virtual (observer) microphone (ear location) by using the VM based FxLMS algorithm.

The block diagram of the VM based FxLMS algorithm is shown in Figure 2, where $P(s)$, $S(s)$, and $\widehat{S}(z)$ are the primary path, the secondary path, and the secondary path model, respectively. The subscript v in $P_v(s)$, $S_v(s)$, and $\widehat{S}_v(z)$ represents the virtual path. Also $W(z)$ is the digital control filter which can be updated at every iteration with the FxLMS algorithm and $\widehat{V}(z)$ the digital response difference between the error microphone and the virtual microphone when a secondary source generates white noise. As the secondary path model $\widehat{S}(z)$ and the virtual secondary path model $\widehat{S}_v(z)$ are implemented as FIR filters, $\widehat{V}(z)$ is also designed as an FIR filter. The exactness of the model $\widehat{V}(z)$ is important in minimizing the error signal for the fast adaptation of the algorithm. The process inside of the dashed line in Figure 2 is the digital part that is worked in a DSP and the outside of the dashed line is the analogue part. The reference signal $x(t)$ with narrowband property is converted to the form of the discrete reference signal $x(n)$ after passing through the ADC (analogue-to-digital converter)—frequency estimation—Sine and Cosine (wave generator) as illustrated in Figure 2. The summation of the disturbance $d(t)$ and the plant output signal $y(t)$ at the error microphone is the error signal which is given as $e(t) = d(t) + y(t)$. Also the virtual error signal at the virtual (observer) microphone can be written by $e_v(t) = d_v(t) + y_v(t)$.

As presented in Figure 2, the VM based FxLMS algorithm relocates the zone of quiet to the observer (virtual) microphone from the error microphone. Thus the virtual error signal $e_v(t)$ at the listener's ear position is necessary to operate the VM based FxLMS algorithm. However it is impossible to obtain the virtual error signal $e_v(t)$ from the listener's ear in the real-time control of a practical active headrest system; the virtual error signal must be estimated

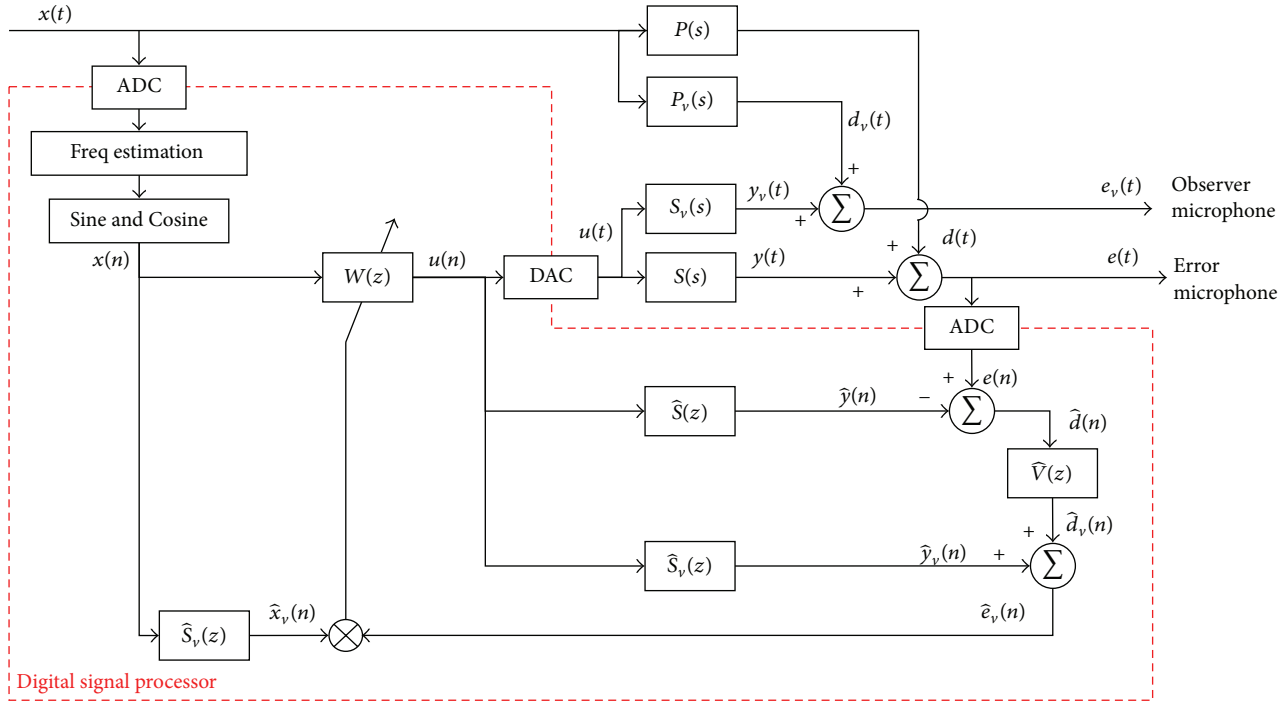

Figure 2: Block diagram of the VM based FxLMS algorithm.

in the algorithm. This aspect is the main difference between the FxLMS algorithm and the VM based FxLMS algorithm in such an active headrest system.

Assuming that the half (left or right) side of the active headrest system has K reference signals, M secondary loudspeakers, and L error microphones, the local gradient of the cost function J with respect to the filter coefficients of each control filter can be expressed as [2]

$$\frac{\partial J}{\partial \mathbf{w}(n)} = \frac{\partial \widehat{\mathbf{e}}_v^T(n)\,\widehat{\mathbf{e}}_v(n)}{\partial \mathbf{w}(n)} = 2\widehat{\mathbf{X}}_v^T(n)\,\widehat{\mathbf{e}}_v(n). \tag{1}$$

Thus the multichannel VM based FxLMS update equation to relocate the active quiet zone to the ear can be given as [2, 8]

$$\mathbf{w}(n+1) = \mathbf{w}(n) - \alpha\widehat{\mathbf{X}}_v^T(n)\,\widehat{\mathbf{e}}_v(n), \tag{2}$$

where $\widehat{\mathbf{X}}_v(n)$ is the filtered-reference signal matrix from the model of the virtual secondary path and can be written by

$$\widehat{\mathbf{X}}_v(n) = \begin{bmatrix} \widehat{\mathbf{x}}_{v1}^T(n) & \widehat{\mathbf{x}}_{v1}^T(n-1) & \cdots & \widehat{\mathbf{x}}_{v1}^T(n-I+1) \\ \widehat{\mathbf{x}}_{v2}^T(n) & \widehat{\mathbf{x}}_{v2}^T(n-1) & \cdots & \widehat{\mathbf{x}}_{v2}^T(n-I+1) \\ \vdots & \vdots & \ddots & \vdots \\ \widehat{\mathbf{x}}_{vL}^T(n) & \widehat{\mathbf{x}}_{vL}^T(n-1) & \cdots & \widehat{\mathbf{x}}_{vL}^T(n-I+1) \end{bmatrix}, \tag{3}$$

where I is the length of $\mathbf{w}(n)$ and $\widehat{\mathbf{x}}_l(n)$ is the virtual filtered-reference signal vector and can be presented as

$$\widehat{\mathbf{x}}_{vl}(n) = \left[\widehat{x}_{v11\ell}(n)\ \ \widehat{x}_{v12\ell}(n)\ \cdots\ \widehat{x}_{v1K\ell}(n)\ \ \widehat{x}_{v21\ell}(n)\ \cdots\ \widehat{x}_{vMK\ell}(n)\right]^T. \tag{4}$$

Also the estimated virtual error signal vector $\widehat{\mathbf{e}}_v(n)$, in (2), at the virtual microphone cannot be directly measured in real-time during control and thus must be estimated, as shown in Figure 2, by

$$\widehat{\mathbf{e}}_v(n) = \widehat{\mathbf{d}}_v(n) + \widehat{\mathbf{y}}_v(n), \tag{5}$$

where $\widehat{\mathbf{d}}_v(n)$ is the estimated virtual disturbance signal vector and is obtained after the estimated disturbance signal, $\widehat{\mathbf{d}}(n)$, passes through the virtual path model $\widehat{V}(z)$ which is defined as the response difference between the error microphone and the observer (virtual) microphone.

By (2), the estimated virtual error signal vector $\widehat{\mathbf{e}}_v(n)$ tends to be zero since $\widehat{\mathbf{y}}_v(n)$ gradually becomes the relevant antinoise that has the same amplitude and the inverse phase of $\widehat{\mathbf{d}}_v(n)$. Thus the zone of quiet can be relocated at the position of the observer (virtual) microphones as illustrated in Figure 1.

3. Experimental Setup

3.1. Active Headrest. As displayed in Figure 3 the block diagram of an active headrest system for the VM based FxLMS algorithm, a primary loudspeaker (Mercury MX2-M), two secondary loudspeakers (Sammi SR-100A), and two error microphones (1/2″ PCB 337B02) are installed around the head and torso simulator (B&K Type 4128-C, HATS) (see Figure 4). In addition, two observer (virtual) microphones (B&K Type 4158-C) are mounted inside of the HATS ears and used just for modelling the virtual secondary paths, $\widehat{S}_v(z)$, and measuring control results. The physical horizontal distance

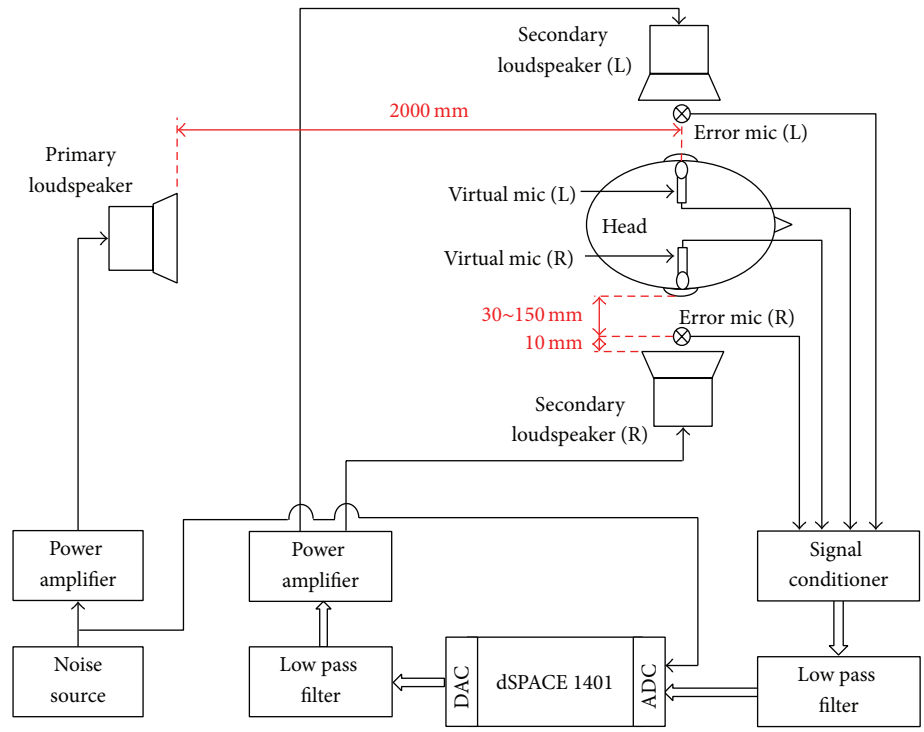

Figure 3: Schematic diagram of the active headrest system for control experiment.

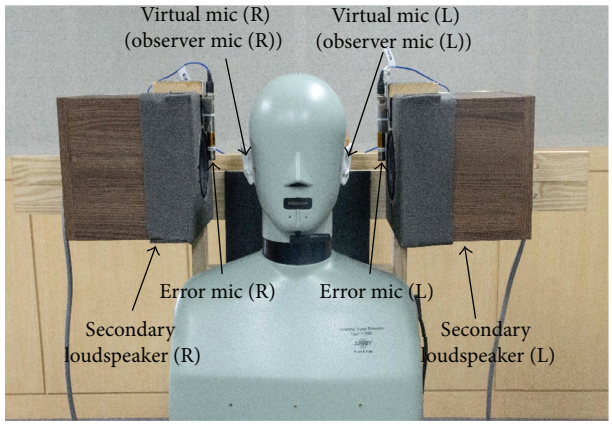

Figure 4: Implementation of the active headrest system.

between the primary loudspeaker and the error microphone or the observer microphone was 2000 mm. The distance Δ between the observer microphone and the error microphone, which was fixed with the secondary loudspeaker at the distance of 10 mm, was varied from 30 to 150 mm with the interval of 30 mm for the measurement of the quiet zone relocation. Thus the distances were $\Delta = 30, 60, 90, 120$, and 150 mm.

For the implementation of the real-time VM based FxLMS for the active headrest, a dSPACE 1401 is used as an embedded controller with some other electronics and circuits including the low pass filters with the cutoff frequency of about 2 kHz for antialiasing and reconstruction filtering of the signals, two signal conditioners (PCB 480E09), and a power amplifier as shown in Figure 3. The sampling frequency was 10 kHz in the real-time control of the headrest system.

The primary noise was a linearly swept narrowband signal with four-component orders of the fundamental frequency C1 (200 → 320 Hz), C1.5 (300 → 480 Hz), C2 (400 → 640 Hz), and C2.5 (500 → 800 Hz). The primary noise which is generated by the powertrain of a passenger car is considered in this study. The noise is a critical problem of such a car and is composed of multiple orders of a sinusoidal wave. The first four orders C1, C1.5, C2, and C2.5 which are the largest contribution of the interior noise are investigated. The noise signal held the lowest frequencies for 3 seconds at the beginning and was swept for 10 seconds at the next step and then maintained the highest frequencies for 2 seconds.

3.2. Secondary Path Modelling. As shown in Figure 2, the active headrest system requires the digital models for the secondary path (secondary loudspeaker, near error microphone) $\widehat{S}(z)$ and the virtual secondary path (secondary loudspeaker, near observer microphone) $\widehat{S}_v(z)$, for the implementation of the VM based FxLMS algorithm in dSPACE 1401. The two secondary paths were implemented as impulse response functions (IRF) $\widehat{s}(n)$ and $\widehat{s}_v(n)$, respectively. By the way the cross secondary path (secondary loudspeaker, opposite error microphone) and the cross virtual secondary path (secondary loudspeaker, opposite observer microphone) were ignored in the control algorithm since they are very small compared to the secondary path and the virtual secondary path, respectively, as plotted in Figure 5.

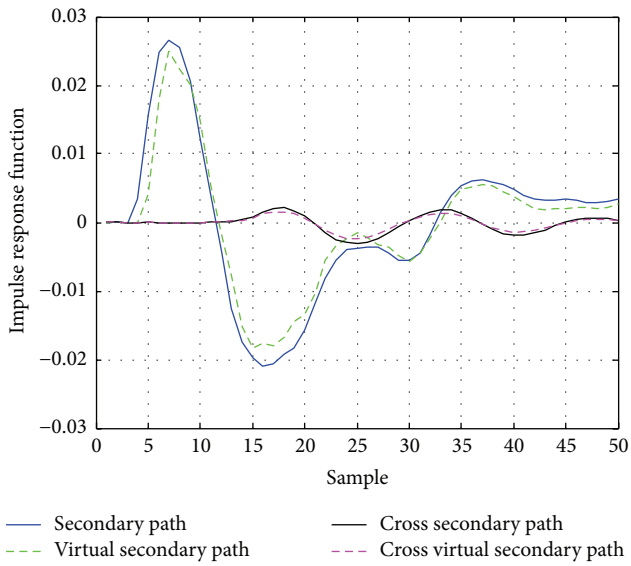

FIGURE 5: Impulse response functions of the secondary, virtual secondary, cross secondary, and cross virtual secondary paths at the distance $\Delta = 30$ mm.

4. Experiment Results and Discussions

4.1. Performance Comparison of FxLMS and VM Based FxLMS. In the real-time control experiment, the two ANC algorithms of the FxLMS and the VM based FxLMS were considered for the active headrest system.

In Figures 6(a) and 6(b), the power spectral densities (PSDs) before and after control, $S_{ee,\text{before}}(f)$ and $S_{ee,\text{after}}(f)$, and the attenuation, $A(f) = 10\log_{10}[S_{ee,\text{after}}(f)/S_{ee,\text{before}}(f)]$, of the *error signal* $e(t)$, as shown in Figure 2, measured at the *error microphone* are plotted, respectively, when the *FxLMS algorithm* is applied in the headrest system. Both plots show the responses after control are similar when the distances Δ between the error microphone and the observer (virtual) microphone are 30, 60, 90, 120, and 150 mm. As the frequency range of the narrowband primary noise with the four orders (C1, C1.5, C2, and C2.5) is 200–800 Hz, the plots are dominant at the frequency range. The amounts of the averaged noise attenuation levels after control are about 14–31 dB over the frequency range regardless of the variation of $\Delta = 30$–150 mm as shown in Figure 6 since the quiet zones are produced at the error microphone positions by the FxLMS algorithm.

In Figures 7(a) and 7(b), the PSDs, $S_{e_ve_v,\text{before}}(f)$ and $S_{e_ve_v,\text{after}}(f)$, and the attenuation, $A_v(f) = 10\log_{10}[S_{e_ve_v,\text{after}}(f)/S_{e_ve_v,\text{before}}(f)]$, of the *observer* signal $e_v(t)$, as shown in Figure 2, measured at the *observer microphone* (ear position) are displayed, respectively, when the *FxLMS algorithm* is implemented. In this case, the noise attenuation levels after control are dramatically decreased by the increase of the distance Δ. Since the location of the quiet zone is centered at the error microphone, the increase of the distance Δ indicates the observer microphone is away further from the center of the quiet zone as explained in Figure 1. Hence the amounts of the averaged attenuation levels at $\Delta = 30$, 60, 90, 120, and 150 mm are about 12, 6, 4, 2, and 1 dB, respectively, as illustrated in Figure 7. This implies the increased Δ causes less reduction at the observer microphone in control.

In Figures 8(a) and 8(b), the PSDs, $S_{ee,\text{before}}(f)$ and $S_{ee,\text{after}}(f)$, and the attenuation, $A(f)$, of the *error signal* $e(t)$ measured at the *error microphone* are plotted, respectively, when the *VM based FxLMS algorithm* is applied. Both plots show the responses after control are greatly different when the distance Δ varies. The noise attenuation levels after control are dramatically decreased or even enhanced by the increase of the distance Δ. Since the center of the relocated quiet zone is the observer microphone (ear position), the increase of the distance Δ indicates the error microphone is away further from the center of the relocated quiet zone as explained in Figure 1.

In Figures 9(a) and 9(b), the PSDs, $S_{e_ve_v,\text{before}}(f)$ and $S_{e_ve_v,\text{after}}(f)$, and the attenuation, $A_v(f)$, of the *observer* signal $e_v(t)$ measured at the *observer microphone* (ear position) are displayed, respectively, when the *VM based FxLMS algorithm* is implemented. Both plots show the responses after control are quite different when the distance Δ varies. The noise attenuation levels after control are gradually decreased by the increase of the distance Δ. Although the virtual secondary paths $\widehat{S}_v(z)$ at each distance Δ are modelled and implemented in the VM based FxLMS at the corresponding control experiment, the attenuation levels become worse by the increase of Δ as shown in Figure 9(b). This is because $\widehat{S}_v(z)$ with the larger Δ contains the larger inaccuracy in the modelling of the actual path $S_v(z)$. The amounts of the averaged attenuations at the distance $\Delta = 30$, 60, 90, 120, and 150 mm are about 20, 22, 19, 15, and 8 dB, respectively. This implies the VM control technique provides further reduction at the observer microphone position in control than the simple FxLMS algorithm.

4.2. Averaged Attenuation Levels around Quiet Zones. In Figures 10 and 11, the amounts of the averaged attenuation levels, $A(f)$ and $A_v(f)$, of the measured signals by the error microphone and the observer microphone around the quiet zones after control with both the FxLMS and the VM based FxLMS algorithms, respectively, against the distances $\Delta = 30$, 60, 90, 120, and 150 mm are outlined. The solid and dotted lines denote the averaged attenuation levels at the error and observer microphones, respectively.

As shown in Figure 10, after the FxLMS control, the amounts of the averaged $A(f)$ measured at the error microphones are about 23-24 dB regardless of the variation of Δ and this is also plotted in Figure 6(b) and discussed in Section 4.1. On the other hand, the amounts of the averaged $A_v(f)$ measured at the observer microphones are steadily worse from 12 dB to 1 dB with the increase of Δ. In addition, the differences between the averaged $A(f)$ and $A_v(f)$ vary from 11 dB at $\Delta = 30$ mm to 22 dB $\Delta = 150$ mm. Hence, in the FxLMS algorithm, the increased Δ causes the less averaged $A_v(f)$ and the increased difference between the averaged $A(f)$ and $A_v(f)$. It is worthy to note that 6 dB of the averaged $A_v(f)$ is achieved at about the distance $\Delta = 60$ mm. Assuming the shape of the quiet zone is a sphere, it is meaningful as the Δ value can indicate the radius of the quiet

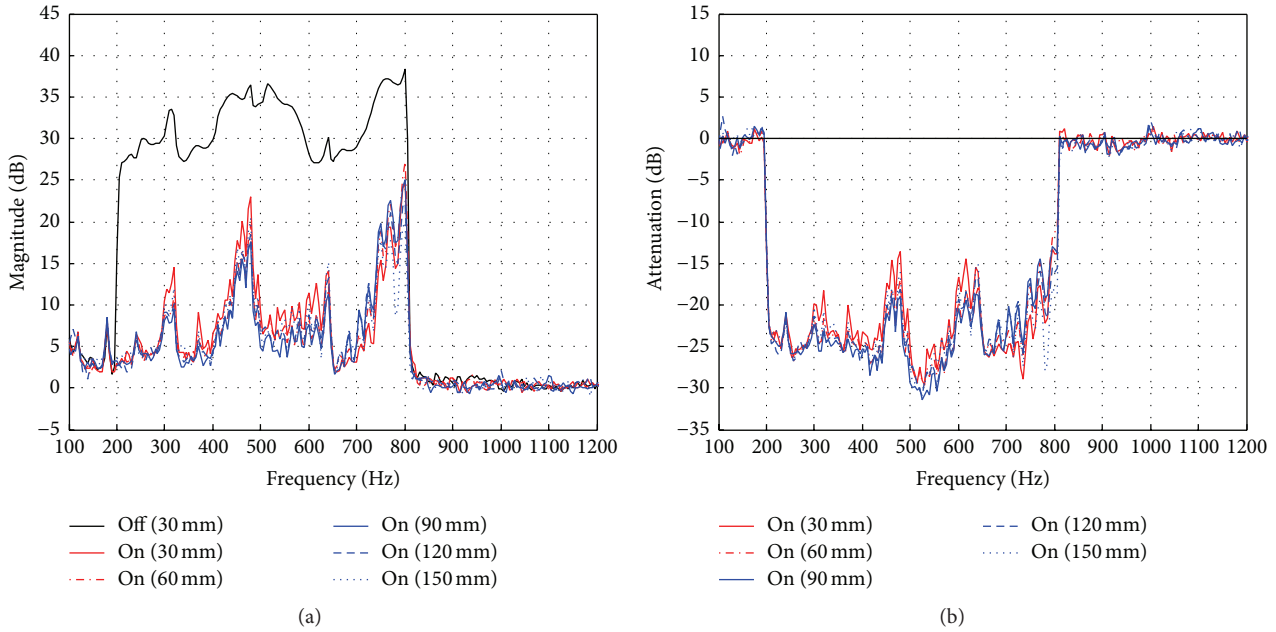

FIGURE 6: Comparison of the measured error signals at the error microphones with the FxLMS algorithm. (a) PSD functions. (b) Attenuations.

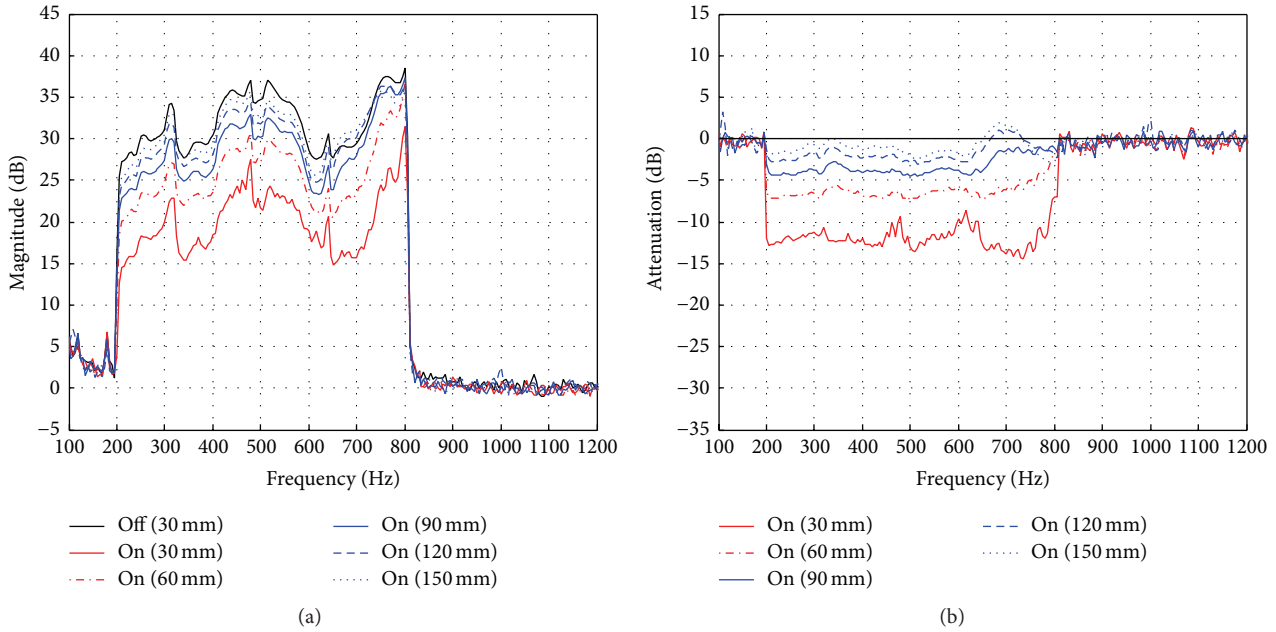

FIGURE 7: Comparison of the measured error signals at the observer (virtual) microphone with the FxLMS algorithm. (a) PSD functions. (b) Attenuations.

zone. The 6 dB attenuation radius of the quiet zone is about 60 mm in this active headrest system against the narrowband primary noise with the FxLMS algorithm.

As displayed in Figure 11, after control with the VM based FxLMS algorithm, the amounts of the averaged $A_v(f)$ (dotted line) measured at the observer microphones are about 8–22 dB by the variation of Δ as the averaged $A_v(f)$ is gradually worse with the increase of the distance Δ although the corresponding virtual secondary path model $\widehat{S}_v(z)$ at each distance is applied in the algorithm. Likewise the averaged $A(f)$ (solid line) measured at the error microphones is steadily worse with the increase of Δ. It is notable that the enhancement is measured by the error microphone position with the distance $\Delta = 80$ mm when the amount of the averaged attenuation at the observer microphone (ear position) is 20 dB. This implies that if a listener at the active headrest system moves his/her ear toward the error microphone under the VM based FxLMS algorithm, he/she will hear even louder noise

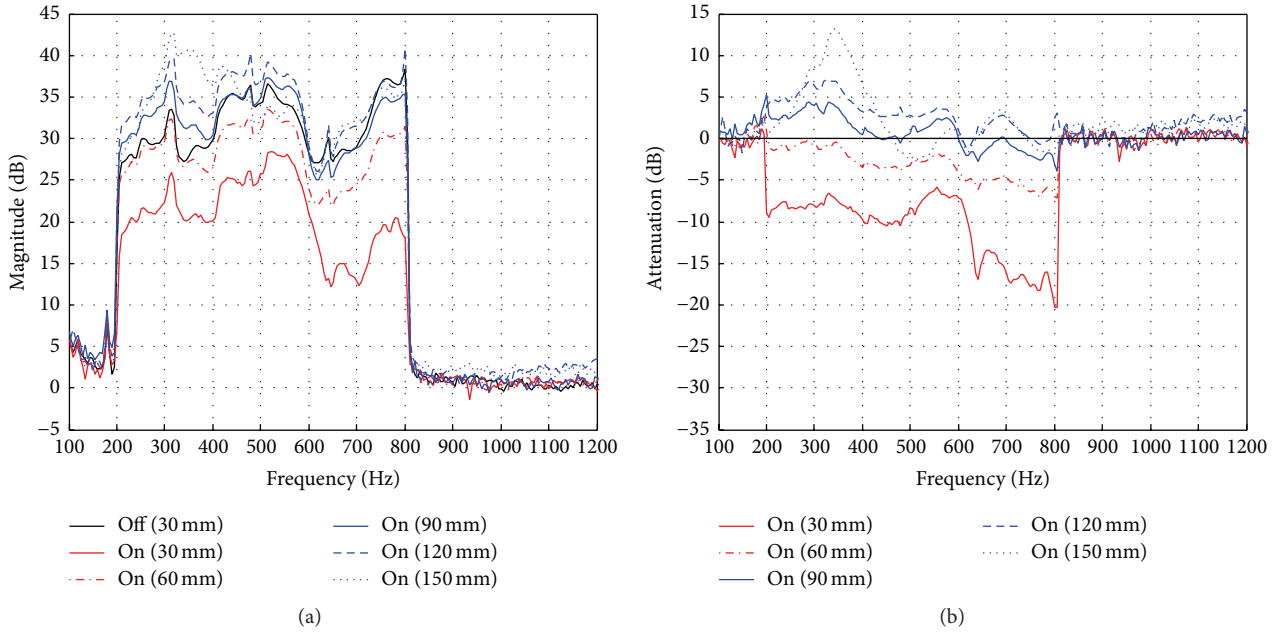

Figure 8: Comparison of the measured error signals at the error microphones with the VM based FxLMS algorithm. (a) PSD functions. (b) Attenuations.

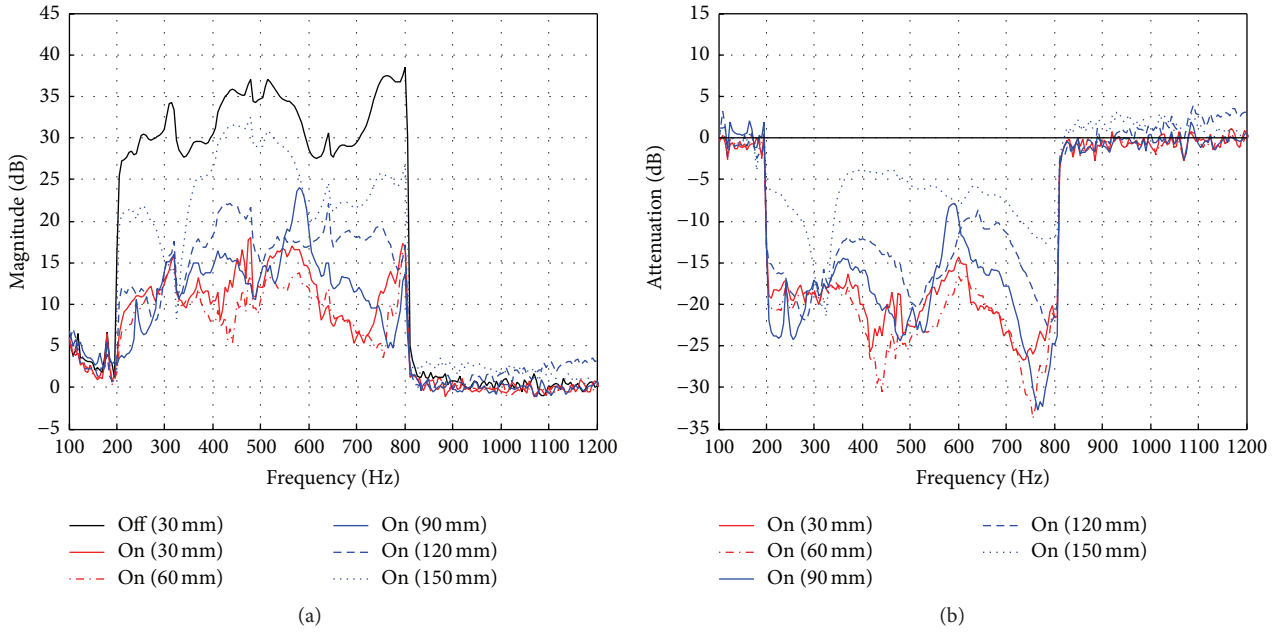

Figure 9: Comparison of the measured error signals at the observer (virtual) microphone with the VM based FxLMS algorithm. (a) PSD functions. (b) Attenuations.

compared to the noise before control. Because of this reason, thus, the allowable head movement range of the listener may be restricted in a practical active headrest system.

For the extension of the quiet zones, it is necessary to have even more exact and precise models of the secondary path and the virtual secondary path. Also more error microphones and secondary loudspeakers can provide further reduction of noise in the headrest system.

In summary of the above discussions, the accuracy of the path models of $\widehat{S}(z)$, $\widehat{S}_v(z)$, and $\widehat{V}(z)$ is important to estimate $\widehat{\mathbf{e}}_v(n)$ in the VM based FxLMS algorithm. Then the algorithm allows achieving reasonable attenuations with proper stability

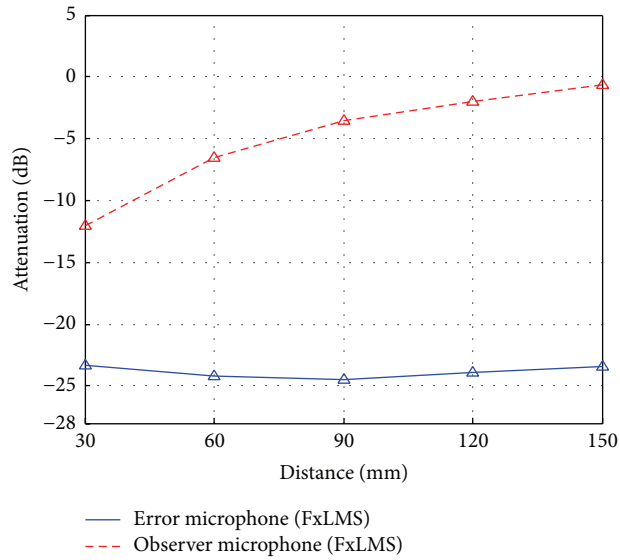

FIGURE 10: Comparison of the averaged attenuations of the measured signals at the error microphone and the observer microphone against the distance Δ with the FxLMS algorithm.

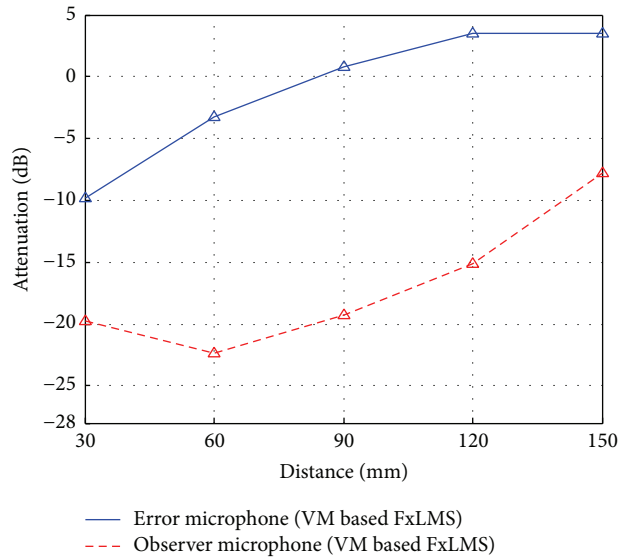

FIGURE 11: Comparison of the averaged attenuations of the measured signals at the error microphone and the observer microphone against the distance Δ with the VM based FxLMS algorithm.

at the listener's ear position in the practical applications such as an active headrest system.

5. Conclusions

This investigation describes a new VM based FxLMS algorithm which can be embedded in a real-time digital controller for an active headrest system. The main outcomes are summarized in the following.

Different from the FxLMS algorithm, the averaged attenuation $A_v(f)$ at the ear position (measured by the observer microphone) achieved was about 8 dB at $\Delta = 150$ mm and 22 dB at $\Delta = 60$ mm under the VM based FxLMS algorithm. The amount of $A_v(f)$ was decreased with the increase of the distance Δ.

The suggested VM based FxLMS algorithm requires the path models of $\widehat{S}(z)$, $\widehat{S}_v(z)$, and $\widehat{V}(z)$ and the accuracy of these models is important to estimate $\widehat{\mathbf{e}}_v(n)$. Then the algorithm allows achieving reasonable attenuations with proper stability at the listener's ear position in the headrest system.

Extending the quiet zones in the active headrest will be considered in terms of multiple error microphones and loudspeakers for the application of real headrest systems in the future.

Competing Interests

The authors declare that they have no competing interests.

Acknowledgments

This research was supported by a grant (12-TI-C01) from the Advanced Water Management Research Program funded by Ministry of Land, Infrastructure and Transport of Korean government.

References

[1] J. Diaz, J. M. Egaña, and J. Viñolas, "A local active noise control system based on a virtual-microphone technique for railway sleeping vehicle applications," *Mechanical Systems and Signal Processing*, vol. 20, no. 8, pp. 2259–2276, 2006.

[2] S. J. Elliott, *Signal Processing for Active Control*, Academic Press, 2001.

[3] S. M. Kuo and D. R. Morgan, *Active Noise Control Systems: Algorithms and DSP Implementations*, John Wiley & Sons, New York, NY, USA, 1996.

[4] J. Kim, Y. Choi, and Y.-S. Lee, "Spectrogram image analysis of error signals for minimizing impulse noise," *Journal of Sensors*, vol. 2016, Article ID 4935694, 9 pages, 2016.

[5] S. J. Elliott, I. M. Stothers, P. A. Nelson, A. M. McDonald, D. C. Quinn, and T. Saunders, "The active control of engine noise inside cars," in *INTER-NOISE and NOISE-CON Congress and Conference Proceedings (InterNoise '88)*, vol. 1998, no. 3, pp. 987–990, Avignon, France, 1988.

[6] S. J. Elliott and A. David, "A virtual microphone arrangement for local active sound control," in *Proceedings of the 1st International Conference on Motion and Vibration Control*, pp. 1027–1031, September 1992.

[7] A. Roure and A. Albarrazin, "The remote microphone technique for active noise control," in *INTER-NOISE and NOISE-CON Congress and Conference Proceedings*, vol. 1999, no. 5, pp. 1233–1244, Fort Lauderdale, Fla, USA, 1999.

[8] M. Pawelczyk, "Multiple input-multiple output adaptive feedback control strategies for the active headrest system: design and real-time implementation," *International Journal of Adaptive Control and Signal Processing*, vol. 17, no. 10, pp. 785–800, 2003.

[9] D. Moreau, B. Cazzolato, A. Zander, and C. Petersen, "A review of virtual sensing algorithms for active noise control," *Algorithms*, vol. 1, no. 2, pp. 69–99, 2008.

[10] M. Pawelczyk, "Multi-channel virtual-microphone feedback minimum-variance active noise control system," *Mechanics*, vol. 28, no. 1, pp. 12–17, 2009.

[11] D. P. Das, D. Moreau, and B. Cazzolato, "Performance evaluation of an active headrest using the remote microphone technique," in *Proceedings of the Annual Conference of the Australian Acoustical Society*, Gold Coast, Australia, 2011, Paper Number 69.